Mon. Not. R. astr. Soc. (1989) **240,** 349–372

High-luminosity *IRAS* galaxies – II. Optical spectroscopy, modelling of starburst regions and comparison with structure

K. J. Leech,[1,2,3] M. V. Penston,[2] R. Terlevich,[2]
A. Lawrence,[3] M. Rowan-Robinson[3] and J. Crawford[3]

[1] *Astronomy Centre, University of Sussex, Falmer, Brighton BN1 9QH*
[2] *Royal Greenwich Observatory, Herstmonceux Castle, Hailsham, East Sussex BN27 1RP*
[3] *School of Mathematical Sciences, Queen Mary College, Mile End Road, London E1 4NS*

Accepted 1989 March 3. Received 1989 March 3; in original form 1988 September 23

Summary. We have obtained moderate-resolution spectrophotometry, and here present various emission-line ratios and emission-line luminosities, for a complete sample of (predominantly high-luminosity) *IRAS* galaxies. Line ratio diagnostic diagrams show most to exhibit H II region-like spectra, although about 12 per cent are Seyferts or LINERs. The fraction of active galaxies does not appear to be a function of IR luminosity. The typical extinction, as derived from Hα/Hβ, is $A_v \approx 1$. Comparison of the [O III]/Hβ line ratios of *IRAS* galaxies with those of an optically selected sample of H II region-like galaxies shows the *IRAS* galaxies to be of lower ionization, which may be due to either higher metallicities or their high dust content. The *IRAS* galaxies show a range of optical colours, with the majority having colours similar to Sc galaxies. Some galaxies, however, have colours indicative of AGN. Comparison with population synthesis models enables us to estimate the number of O stars present, which is consistent with the observed emission-line flux. The IR to emission-line luminosity ratio of all the *IRAS* galaxies is, however, very high, suggesting a much higher optical depth. We reconcile these observations by presenting a simple model with two types of region: Type I clouds representing very recent star-formation with $A_v \approx 20$, and Type II clouds with $A_v \approx 1$, representing older starburst and/or general disc star-formation.

1 Introduction

While *IRAS*, the *Infra-Red Astronomical Satellite,* detected many normal, low-luminosity galaxies (de Jong *et al.* 1984; Lawrence *et al.* 1986), it also discovered a new class of galaxies with IR luminosities comparable to the bolometric luminosities of quasars (Soifer *et al.* 1984a,b; Allen, Roche & Norris 1985; Lawrence *et al.* 1986). These galaxies are

predominantly spirals. Most of their energy is emitted in the IR and they are approximately 10 times more common than Seyferts at the same IR energy output (Lawrence *et al.* 1986), possibly equally common at the same bolometric output (Soifer *et al.* 1986). Most *IRAS* galaxies have H II region-like spectra, suggesting star formation as the dominant energy source (Allen *et al.* 1985; Elston, Cornell & Lebofsky 1985; Rowan-Robinson & Crawford 1986; Leech *et al.* 1988), although the *IRAS* data have also been used to discover many new Seyfert galaxies (de Grijp *et al.* 1985; Carter 1985; de Robertis & Osterbrock 1985). Possible triggers of star formation include interactions with companion galaxies – Allen *et al.* (1985) found 68 per cent of a sample of 19 optically faint *IRAS* galaxies were disturbed, interacting or had close companions, while Saunders *et al.* (1986), from a sample of 15 high-luminosity sources, concluded that the majority, if not all, of the most-luminous *IRAS* galaxies were interacting systems. Gas transfer along the bars of spiral galaxies is also thought to trigger star formation (Hawarden *et al.* 1986). Dust-obscured Active Galactic Nuclei (AGN) (Norris *et al.* 1985; de Poy, Becklin & Wynn-Williams 1986; Becklin 1986), and direct mechanical heating of gas and dust in galaxy–galaxy collisions (Harwit *et al.* 1987), are two alternative theories of the high-luminosity galaxies. For 10 galaxies with far-IR luminosity $>10^{12}L_{\odot}$, Sanders *et al.* (1988) concluded that all were interacting or merging, and all but one showed spectra characteristic of active nuclei (Seyferts or LINERs).

To study the relative importance of star formation and Seyfert activity for the *IRAS* galaxy phenomenon and to see what fraction of *IRAS* galaxies are interacting, we obtained CCD images and IPCS spectra for a complete sample of high-luminosity *IRAS* galaxies. The CCD images enable us to calculate the fraction of interacting galaxies and see how this fraction changes with IR luminosity. Results are presented in an accompanying paper (Lawrence *et al.* 1989, Paper I). The present paper gives the results of medium-resolution spectrophotometry, discusses them in terms of line ratio diagrams, compares the *IRAS* galaxy spectral and morphological classifications, and compares the *IRAS* galaxies with optically selected starburst galaxies. We then discuss optical colours, the ratio of IR to line emission and the implications these have for the 'starburst' interpretation. We present a 'two cloud' starburst model which can explain the data consistently.

2 An objective sample of high-luminosity *IRAS* galaxies

An objective way to sample the high IR luminosity galaxies discovered by *IRAS* is required. We decided to study a subset of the Lawrence *et al.* (1986) sample of north galactic pole *IRAS* galaxies. The latter was a sample of 496 *IRAS* sources with $S_{60\mu m}>0.5$ Jy, $b>60°$, and away from the Virgo cluster. Redshifts for all except 3 out of 237 galaxies with a 60-μm flux density greater than 0.85 Jy were obtained, and $L_{60\mu m}$ luminosities were calculated assuming $H_0=50$ km s^{-1} Mpc^{-1} and $\Omega=1$. In order to reduce the Lawrence *et al.* sample to a manageable number and to concentrate on the higher-luminosity sources, a subset was selected using the following criteria: $z>0.01$, with a high-luminosity sub-sample defined by $L_{60\mu m}>10^{11.5}L_{\odot}$, $S_{60\mu m}>1$ Jy and a low-luminosity sub-sample defined by $L_{60\mu m}<10^{11.5}L_{\odot}$, $S_{60\mu m}>2$ Jy.

These criteria were used to select 61 sources. The reason for the two flux limits is to give us a sufficient number of high IR luminosity galaxies without allowing the low IR luminosity (nearby) galaxies to dominate the sample. The redshift lower limit was primarily intended to ensure that the optical image of every galaxy would fit onto a CCD chip, but also concentrates the sample to higher luminosities. The sample is meant to be 'self controlling', in that it contains low IR luminosity sources with which the properties of the high-luminosity ones may be compared. In the case of interacting galaxies, a source may be associated with more than one galaxy.

The sample sources are listed in Table 1, along with optical synonyms and references to earlier observations. A figure comparing the luminosity distribution of our new sample with the complete $S_{60\mu m} > 0.5$ Jy flux-limited Lawrence *et al.* sample, and Shapley-Ames galaxies in the same area is shown in Paper I.

2.1 OBSERVATIONS AND DATA REDUCTION

Spectroscopic observations of the sample galaxies were carried out at the Observatorio del Roque de los Muchachos (La Palma) using the Intermediate Dispersion Spectrograph and the IPCS detector at the Cassegrain focus of the Isaac Newton Telescope (INT) between 1986 May 31 and June 6. A slit 1.5 arcsec wide was used, kept at the parallactic angle to reduce the effects of differential atmospheric refraction. The weather was mostly photometric, with seeing

Table 1. Previous observations of sample galaxies.

Name	Alternative Optical Name(s)	Notes
12590+2934	NGC 4922A+B, UGC 8135, MCG 5-31-99, ZG 1259+29.	Smith. Classified as Seyfert 2 by VCV
13005+3556		
13086+2950	NGC 5004C, UGC 8259, MCG 5-31-150, ZG 1308+29.	Smith.
13111+4348		
13126+2452	MCG 4-31-15, ZG 1312+24.	Smith.
13183+3423	IC 883, UGC 8387, ZG 1318+34, Arp 193, I ZW 56.	
13238+3611	NGC 5149, UGC 8444, MCG 6-30-010, ZG 1323+36.	
13254+4754		
13326+3417	UGC 8561, MCG 6-30-46, ZG 1332+34.	
13342+3932		
13362+4831		2 nuclei, Seyfert 2 and Liner; M,VCV
13376+2839	NGC 5263, UGC 8648, MCG 5-32-58, ZG 1337+28.	Smith.
13387+2331	MCG 4-32-25, ZG 1338+23.	Smith.
13387+2951		
13408+3035	UGC 8685, MCG 5-32-74, ZG 1340+30.	
13442+2321		
13457+3513		
13470+3530	UGC 8739, MCG 6-30-90, ZG 1347+35.	
13532+2517		Smith.
13536+1836	UGC 8850, MCG 3-36-5, ZG 1353+18, MKN 463.	Seyfert 2; M, dG, VCV
13539+3019	UGC 8856, ZG 1354+30, MCG 5-33-21.	Smith.
13539+2920		
13564+3741	NGC 5394, UGC 8898, MCG 6-31-33, ZG 1356+37, Arp 84, VO48B.	
13565+3519	MCG 6-31-36.	
13573+2517		
13589+4305	MCG 7-29-36.	
13592+3107		
14003+3245	NGC 5433, UGC 8954, MCG 6-31-50, ZG 100+32.	
14008+2816	UGC 8961, MCG 5-33-42.	Smith.
14026+3058	MCG 5-33-46, ZG 1402+30.	Smith.
14046+3400	MCG 6-31-070, ZG 1404+34.	
14048+1524	MCG 3-36-49, ZG 1404+15.	
14057+3227		
14060+2919		
14082+1347	ZG 1408+13.	Seyfert 2; dG
14096+2428		
14124+1522	NGC 5522, UGC 9116, MCG 3-36-89, ZG 1412+15.	
14144+3949	NGC 5541, UGC 9139, MCG 7-29-59, ZG 1414+39.	

Table 1 – *continued*

14151+2705	UGC 9141, MCG 5-34-7, ZG 1415+27, MKN 673.	Smith. Seyfert 2; M.
14158+2741		Smith.
14165+2510	UGC 9165, ZG 1416+25, MCG 4-34-15.	Smith.
14178+4927	ZG 1417+49, MKN 1490.	M, VCV.
14202+2615		
14203+3005		
14221+2450	NGC 5610, UGC 9230, MCG 4-34-25, ZG 1422+24.	Smith.
14228+1358	UGC 9239, ZG 1422+13.	
14229+1424		
14271+4203	UGC 9307, MCG 7-30-16, ZG 1427+42.	
14280+3126	NGC 5653, UGC 9318, MCG 5-34-58, ZG 1427+31.	Smith.
14283+3532	NGC 5656, UGC 9332, MCG 6-32-53, ZG 1428+35.	
14296+2209	ZG 1429+22.	
14332+3520	MCG 6-32-70.	
14356+3041	UGC 9425, MCG 5-34-83, ZG 1435+30.	Smith.
14405+2634		
14422+1644		
14434+3859	NGC 5755, U9507, MCG 7-30-63, ZG 1443+38.	
14459+1745		
14471+2333		
14547+2448	UGC 9618, MCG 4-35-18,19 , Arp 302, V 340.	Smith.
14575+3256		
15018+2417		Smith.

Notes: M refers to the Mazzarella & Balzano (1986) catalogue of Markarian galaxies; dG refers to the de Grijp, Miley & Lub (1987) catalogue of warm *IRAS* sources from the PSC thought to be AGN candidates; VCV refers to the Véron-Cetty & Véron (1987) catalogue of active galaxies and quasars. Smith refers to Smith *et al.* (1987), who obtained redshifts of a flux-limited sample of *IRAS* galaxies and used them to construct a luminosity function for *IRAS* galaxies.

between ≈ 0.9 and 1.8 arcsec. The wavelength range used was between 3500 and 7500 Å and the instrumental resolution of two pixels was ≈ 4 Å. Integrations on each object were carried out until it would have been possible to detect a line at the position of [O I] λ6300 with a strength of about 1/20 that of Hα, whether or not a line was detected, or until 2000 s had elapsed. An arc was taken at the same position in the sky after each observation and several photometric standards were observed each night.

Fifty-six out of the 61 sample sources were observed. In the case of sources which were interacting galaxies, both components were observed, and some galaxies were observed more than once, e.g. for a nucleus and an H II region of a galaxy. A total of 79 spectra were obtained. Observations of the sources are almost complete – 24 out of 25 sources with luminosities greater than $10^{11.5} L_{\odot}$ were observed, while 32 out of 36 sources with luminosities below this value were observed.

The data were wavelength- and flux-calibrated using the SPICA data-reduction package. Each spectrum was wavelength-calibrated using its associated arc, had the sky background removed, was corrected for extinction using the standard La Palma extinction corrections, and was then flux-calibrated using the observations of standard stars. A noise spectrum was calculated for each galaxy by adding the sky background noise and the galaxy spectrum noise in quadrature. During data reduction, some spectra with low signal-to-noise ratios were re-binned to either a half or a quarter of the original spectral resolution to improve their S/N ratio. Fig. 1 shows spectra of four sample galaxies: a LINER, a Seyfert 2, an H II region-like galaxy and a galaxy with strong Balmer absorption.

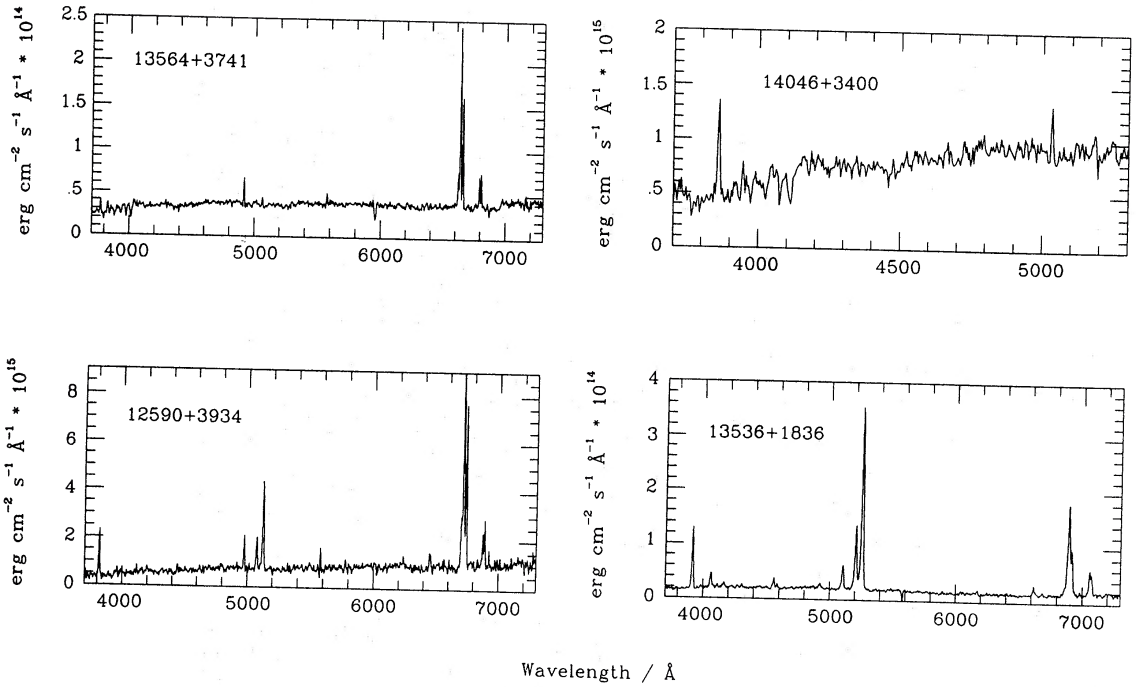

Figure 1. Optical spectra of four typical *IRAS* sources from our sample. 12590+2934 is a LINER, 13536+1836 is a Seyfert 2 and 13564+3741 an H II region-like galaxy. 14060+3400 exhibits Balmer line absorption from A and F stars.

Redshifts for each galaxy were obtained from the weighted means of the redshifts of individual emission lines. The emission lines usually used were Hα, Hβ, [N II]λ6584, [O I]λ6300, [O III]λ5007 and [O II]λ3727. Three galaxies with no immediately obvious emission lines had weak emission lines identified using a preliminary redshift obtained from the Na *D* absorption line. One galaxy, 14224+1358, had no detectable features in its IPCS spectrum. Heliocentric velocities were converted to galactocentric velocities using the standard 300 sin l cos b km s^{-1} correction.

Emission-line fluxes, converted to luminosities using galactocentric redshifts, and absorption-line equivalent widths, were measured using the SPICA EW function. Monochromatic continuum fluxes were measured in erg cm^{-2} s^{-1} Å^{-1} in each galaxy's rest frame at 3700, 4200 and 5700 Å by averaging the continuum flux over a 100 Å range, and at 6560 Å by interpolating the continuum flux under the Hα+[N II] blend from either side of the blend (that is, they were measured at a wavelength of $\lambda(1+z)$ and then multiplied by $(1+z)$ to correct for the stretching effect). Two galaxies have their Hα lines affected by atmospheric absorption. 14202+2615 has a redshift such that Hα lies in the middle of the *A* band, while the Hα line for 14296+2209 lies just to the blue side of the *B* band. The Hα fluxes from these galaxies should be treated with caution.

The photometric accuracy of the spectra is difficult to assess. The counts in the spectra of standard stars vary by up to 30 per cent between the nights, due to variations in the seeing, and the narrow slit used. The emission-line sources may not be point sources; indeed some are clearly extended – it should be remembered that all luminosities are through-slit luminosities. Comparing the Hα luminosities of those galaxies observed during the Faint Object Spectrograph run, reported in Leech *et al.* (1988), with the fluxes derived from the IPCS data, show them to be in agreement within the 30 per cent error estimate. While the luminosities are subject to the above uncertainties, relative fluxes, such as line flux ratios or colours, should have smaller errors.

3 Balmer line stellar absorption correction and reddening correction

3.1 BALMER LINE CORRECTION

Some of the galaxies exhibit Balmer line absorption from an early-type stellar population, usually in the Hβ and Hγ lines, and it is assumed that all the galaxies suffer from this to some extent. The effect of this absorption is to reduce the strength of the higher-order Balmer lines, and this needs to be corrected for while calculating Hβ/Hα emission-line flux ratios used in calculating the reddening, or plotting the galaxies on BPT diagrams (Baldwin, Phillips & Terlevich 1981). Similar corrections are made by other authors, e.g. McCall, Rybski & Shields (1985), who observed 99 H II regions in their study of extragalactic H II regions, obtaining a value of 1.9 Å for the Hβ absorption equivalent width which was applied to all their spectra. Our method of determining this correction is similar to theirs, except that they assumed the early-type stellar population to cause equal absorption in Hβ and Hα, whereas here it is assumed there is effectively no Hα absorption. The reddening curve used in the following calculations was taken from Savage & Mathis (1979).

Two methods were used to estimate the equivalent width of the absorption. The first was by correcting the Hα, Hβ, Hγ and Hδ Balmer lines for stellar absorption until the visual absorption calculated from any pair of lines was identical. For example, the absorption at V calculated from two emission lines i and j is given by

$$A_v = 3.1 \times E(B-V) \times \frac{2.5 \times \log[R_{ij}(f_j/f_i)]}{A_i - A_j}, \tag{1}$$

where A_v is the absorption at V calculated from lines i and j, A_X is the interstellar absorption at line X, f_X is the observed flux in line X and R_{ij} is the theoretical ratio of the lines i and j – Case B recombination values are used for the Balmer lines.

But the line fluxes are affected by stellar absorption. The observed emission-line flux (O), the emitted emission-line flux (f), the equivalent width of Balmer absorption from early-type stars (w_i, for the i^{th} Balmer line) and the continuum flux (C) are related by

$$O_i = f_i - w_i * C_i. \tag{2}$$

C should only be that part of the continuum due to early-type stars, but since we have no way of separating the fraction of early-type star continuum from the late-type star continuum, C is taken to be the entire continuum flux at a particular wavelength. The Hβ, Hγ and Hδ absorption equivalent widths (w) for early-type stars (O to F) are approximately equal and, to a good approximation, Hα is not affected by absorption (O'Connell 1973).

If the value of A_v obtained from equation (1) using the Hα and Hβ emission lines is equated to that obtained from the Hβ and Hγ emission lines, we obtain (after some re-arrangement) the equation:

$$\log(O_\beta + w*C_\beta)\left[\frac{A_\alpha}{E(B-V)} - \frac{A_\gamma}{E(B-V)}\right] = \left[\frac{A_\alpha}{E(B-V)} - \frac{A_\beta}{E(B-V)}\right]$$
$$\times [\log R_{\beta\gamma} + \log(O_\gamma + w*C_\gamma)] + \left[\frac{A_\beta}{E(B-V)} - \frac{A_\gamma}{E(B-V)}\right](\log R_{\beta\alpha} + \log O_\alpha), \tag{3}$$

where α, β and γ refer to the Hα, Hβ and Hγ emission lines. Since w is the only unknown in the above equation, it can be determined numerically. Similarly, Hα, Hβ and Hδ may be used to obtain another estimate of w.

This procedure did not give satisfactory values of w for some galaxies with spectra having poor signal-to-noise ratios. Where it failed, a second, a simpler system was used. In the case of no reddening, we may reduce equation (1) to

$$w=\frac{O_i-R_{ij}O_j}{R_{ij}C_j-C_i}, \tag{4}$$

which is a good approximation over the restricted wavelength range Hβ to Hδ and gives an estimate of the upper limit of stellar absorption.

The average value we found for the Hβ absorption equivalent width, using the second method only when the first one failed, was 4 Å. This corresponds approximately to the value expected for a giant A star – A stars have the strongest Balmer line absorption along the spectral sequence, but dwarfs have stronger absorption lines than giants. This correction increases the strength of the average Hβ line by approximately 100 per cent. The equivalent widths of the Balmer line corrections for individual galaxies are given in Table 2.

The Hβ line is one of the most important emission lines in a galaxy's optical spectrum, since it is not only used to derive certain line-ratios but in the reddening correction of several others. the above correction to Hβ will directly affect any ratios involving the Hβ line, such as the [O III]/Hβ and Hα/Hβ ratios, reducing their value compared to any uncorrected ratios. Any error on the correction will be acting upon a reduced ratio. The Hβ correction also affects the [O II]/[O III] ratio, through the reddening correction, but it will hardly affect the [N II]/Hα and [O I]/Hα ratios.

3.2 REDDENING CORRECTIONS FOR BPT DIAGRAMS

Reddening corrections were made before plotting the galaxies on line ratio diagrams. They were carried out in accordance with the method described in BPT, after correcting for stellar Balmer absorption, and the line ratios are given by (in the notation of BPT):

$$(5007/4861)=\log[I(5007)_{\rm obs}/I(4861)_{\rm corr}]-0.11\log[I(\mathrm{H}\alpha)_{\rm obs}/I(\mathrm{H}\beta)_{\rm corr}]+0.05$$

$$(6584/6563)=\log[I(6584)/I(6563)]_{\rm obs}-0.01\log[I(\mathrm{H}\alpha)_{\rm obs}/I(\mathrm{H}\beta)_{\rm corr}]$$

$$(3727/5007)=\log[I(3727)/I(5007)]_{\rm obs}+0.98\log[I(\mathrm{H}\alpha)_{\rm obs}/I(\mathrm{H}\beta)_{\rm corr}]-0.45$$

$$(6300/6563)=\log[I(6300)/I(6563)]_{\rm obs}+0.12\log[I(\mathrm{H}\alpha)_{\rm obs}/I(\mathrm{H}\beta)_{\rm corr}]+0.05,$$

where $I(\lambda)$ is the observed intensity of the line at wavelength λ, except in the case of Hβ where the Balmer absorption estimate has been used to correct the observed line flux. This reddening correction and its possible errors are discussed in BPT.

The BPT general excitation indicator, $\langle\Delta E\rangle$ is given by

$\langle\Delta E\rangle=[\Delta E(5007/4861)+\Delta E(6584/6563)+\Delta E(6300/6563)]/3$, where $\Delta E(5007/4861)=(5007/4861)+\log(0.32+x)-0.44$, $\Delta E(6584/6563)=\frac{1}{2}[(6584/6563)-\log[x/(x+1.93)]+0.37]$, $\Delta E(6300/6563)=1/5[(6300/6563)+2.23]$

and

$x=(3727/5007)$.

4 The spectral classification of *IRAS* galaxies

Several *IRAS* sources have two or more optical candidates (interacting galaxies, neighbouring non-interacting objects, or chance alignment of galaxies) within the *IRAS* error ellipse. The

Table 2. Galaxy line ratios, observed Hβ equivalent widths and Hβ absorption correction.

Galaxy	$\left(\frac{H\alpha}{H\beta}\right)^1$	$\left(\frac{[OIII]}{H\beta}\right)$	$\left(\frac{[NII]}{H\alpha}\right)$	$\left(\frac{[OI]}{H\alpha}\right)$	$\left(\frac{[OII]}{[OIII]}\right)$	$<\Delta E>$	Obs $H\beta^2$ ew /Å	Hβ Abs^3 ew /Å
12590+2934	0.92	0.48	-0.19	-1.01	0.06	0.39	15.0 ± 4.9	2.0
13005+3556 Plume	0.82	-0.57	-0.30	-1.24	1.01	0.18	6.7 ± 3.0	3.0
13005+3556 Nucleus	0.86	-0.28	-0.36	-1.12	0.78	0.21	4.9 ± 2.9	4.0
13086+2950	0.65	-0.89	-0.28	-1.30	0.29	-0.08	2.4 ± 2.0	5.0:
13111+4348	0.54	0.27	-0.14	-1.62	-0.22	0.29	6.4 ± 2.4	5.0:
13126+2452	0.50	0.62	0.09	0.22	-0.14	0.56	-0.5 ± 1.0	1.0:
13183+3423	0.50	-0.72	-0.18	-0.80	0.59	0.07	-0.1 ± 0.9	7.0:
13238+3611	0.67	-0.80	-0.25	-2.52	0.69	-0.06	2.1 ± 1.3	6.0:
13254+4754	0.46	-0.04	-0.64	-1.64	0.56	0.16	6.3 ± 3.7	4.0:
13326+3417	0.71	-0.35	-0.39	-1.60	0.55	0.10	2.8 ± 1.4	2.5
13342+3932	0.76	0.66	-0.08	-2.06	-0.27	0.40	10.4 ± 3.6	0.0
13362+4831 NE	0.60	0.49	-0.21	-0.91	0.05	0.40	26.0 ± 7.8	0.0
13362+4831 SW	0.61	0.50	-0.32	-1.22	-0.14	0.36	17.0 ± 4.8	5.0
13376+2839	0.67	-0.76	-0.37	-1.74	1.10	0.09	1.3 ± 1.2	4.0:
13387+2331	0.81	0.63	0.12	-0.91	0.16	0.51	4.0 ± 2.6	2.5:
13387+2951	0.95	-0.13	-0.31	-1.23	0.75	0.26	4.9 ± 1.9	2.5:
13408+3035	0.72	-0.64	-0.24	-2.04	0.75	0.04	2.0 ± 1.9	3.0:
13442+2321	0.87	-1.07	0.44	-0.51	1.99	0.48	2.1 ± 3.0	0.0:
13457+3513	0.56	-0.76	-0.44	-1.70	0.78	0.00	4.0 ± 3.7	10.0
13470+3530	0.56	-0.43	-0.52	-1.21	0.46	0.06	10.8 ± 4.3	9.0:
13536+1836	0.68	0.92	-0.43	-1.10	-0.39	0.50	31.2 ± 5.3	0.0
13539+2920	0.89	-0.06	-0.26	-0.99	0.93	0.35	6.0 ± 2.8	5.0
13564+3741	0.65	-0.87	-0.18	-1.70	0.62	-0.03	6.0 ± 1.7	5.0
13565+3319	0.61	-0.46	-0.32	-1.09	0.50	0.10	2.6 ± 2.1	6.0
13573+2517	1.10	-0.04	-0.16	-1.92	1.28	0.41	-1.3 ± 1.5	2.0:
13589+4305	0.84	-0.44	-0.34	-1.24	0.81	0.16	8.3 ± 3.6	2.0
14003+3245	0.59	-0.77	-0.42	-1.56	0.58	-0.03	6.6 ± 2.4	7.0:
14008+2816	1.01	-0.33	-0.20	-0.64	1.06	0.33	0.4 ± 0.8	1.0:
14026+3058	0.53	-0.70	-0.11	-0.88	0.45	0.06	-0.2 ± 0.5	4.0:
14046+3400	0.71	-0.74	-0.31	-2.13	0.95	0.04	3.0 ± 1.5	5.0
14057+3227	0.74	-0.51	-0.38	-1.59	1.00	0.16	5.5 ± 3.3	3.0
14060+2919	0.86	-0.13	-0.49	-1.25	0.76	0.22	16.0 ± 5.6	2.0
14082+1347	0.68	0.34	-0.09	-0.75	-0.15	0.37	0.7 ± 1.1	6.0
14096+2428	-1.37	-1.09	2.01	0.57	-0.78	0.40	0.2 ± 1.2	2.0:
14144+3949	0.56	-0.49	-0.57	-1.95	0.56	0.01	8.1 ± 3.4	3.0:
14151+2705	0.49	-0.64	-0.14	-0.97	0.58	0.09	0.7 ± 1.0	5.0:
14158+2741	0.57	-0.10	0.02	-0.81	0.49	0.29	-0.1 ± 1.0	3.0:
14165+2510	0.56	-0.69	-0.39	-1.17	0.62	0.03	1.7 ± 1.9	10.0:
14178+4927	0.92	-0.46	-0.15	-1.53	0.74	0.15	1.7 ± 1.2	4.0
14202+2615	0.26	-0.02	-0.15	-1.07	0.06	0.23	16.1 ± 4.4	0.0
14203+3005	0.85	0.89	-0.07	-1.03	-0.35	0.55	0.4 ± 0.9	5.0
14221+2450	0.64	-0.17	-0.20	-1.12	0.38	0.20	3.8 ± 3.3	5.0:
14228+1358	0.70	-0.68	0.15	-0.63	1.05	0.26	0.2 ± 0.5	1.0:
14229+1424	0.56	0.49	-0.71	-1.62	-0.26	0.27	37.0 ±11.0	5.0:
14271+4203	-0.90	-0.19	0.47	-0.35	-1.44	0.55	-0.2 ± 0.4	2.0
14280+3126	0.68	-0.70	-0.42	-1.89	0.77	0.01	27.6 ± 6.2	4.0:
14283+3532	1.22	-0.71	-0.44	-0.37	1.37	0.27	0.4 ± 1.0	0.0
14296+2209	0.89	-0.51	-0.43	-1.20	0.77	0.11	5.5 ± 2.4	3.0:
14332+3520	0.50	-0.70	-0.40	-2.14	0.47	-0.07	3.3 ± 1.2	5.0:
14356+3041	0.73	-0.66	-0.34	-1.95	0.88	0.06	9.0 ± 2.0	2.0:
14405+2634	0.63	-0.52	-0.30	-0.89	0.59	0.12	5.9 ± 2.3	3.0:
14422+1644	0.47	-0.54	-0.24	-1.18	0.64	0.11	1.2 ± 1.8	9.0:
14434+3859	0.26	-0.82	-0.18	-1.26	0.64	0.02	-0.5 ± 0.8	5.0:
14471+2333	0.67	-0.94	-0.32	-1.77	1.25	0.08	1.8 ± 2.1	6.0
14547+2448	0.50	-0.74	-0.40	-1.39	0.51	-0.02	5.1 ± 1.7	5.0:
14575+3256	0.78	0.00	-0.28	-1.50	0.48	0.23	24.5 ± 6.5	2.0
15018+2417	0.60	-0.01	-0.13	-1.22	0.36	0.25	1.8 ± 1.6	4.0

Notes: (1) These are base 10 logarithmic line ratios. All, except Hα/Hβ, are calculated after correcting for Balmer line absorption (Section 3.1) and reddening (Section 3.2). The Hα/Hβ ratio is corrected for Balmer line absorption but not reddening. (2) This is the observed Hβ equivalent width uncorrected for reddening or absorption by early type stars. (3) The Hβ abs ew is the equivalent width of the Hβ absorption from early type stars. It is the amount the observed Hβ equivalent width is corrected by.

optical candidate with the strongest Hα emission was chosen as the 'correct' identification, i.e. the galaxy which was thought to be emitting the IR radiation. In cases where the Hα line strengths were similar, the decision was based on which optical candidate was closest to the *IRAS* source position. This procedure was not followed for two sources. 13005+3556 had similar Hα emission from both its nucleus and a ring around the galaxy, while 13362+4831 is a merging system with two nuclei of similar Hα strength. In these two cases, the sources appear twice in the correlation diagrams, assuming that all the IR flux comes from the component under consideration. It must be remembered that, where there are two candidates for a source, the *IRAS* beam usually includes both galaxies.

Table 2 lists various line ratios for individual galaxies along with the Hβ correction, while Table 3 gives the redshifts, luminosities and colours of each of the sample galaxies and notes the active galaxies.

4.1 LINE RATIOS AND LINE RATIO DIAGRAMS

Nearly all the galaxies show emission spectra, and we can use BPT-type criteria to separate H II region-like galaxies from active galaxies. When the best-quality line-ratio data are plotted in correlation diagrams, the galaxies fall into two groups of high- and low-excitation objects. The division is most marked on diagrams using the [O III]/Hβ ratio (e.g. Fig. 2a). The two selection criteria which an object must simultaneously satisfy to be classified as active are (i) $(5007/4861) > 0$, (ii) $\langle \Delta E \rangle > 0.19$. Applications of these criteria to all the galaxies produces a list of 11 'high excitation' galaxy spectra. One galaxy has a very poor quality spectrum and, given the errors, may not be active. We are uncertain as to the classification of two other galaxies. While 13111+4348 is reminiscent of a low, about a third solar, metallicity H II region and 14229+1424 that of a higher, about solar, metallicity H II region, both are on the H II region/active galaxy borderline in the diagnostic diagrams. We believe them to be normal H II region-like galaxies. The remaining eight objects are almost certainly active, which leads to seven active *IRAS* sources, as 13362+4831 is a merging system with both nuclei active.

Seyfert galaxies may be distinguished from LINERs (called shock-excited galaxies in BPT) by the BPT criterion that Seyferts have (3727/5007) smaller than zero, while LINERs have this ratio greater than zero. Table 4 lists the active *IRAS* sources and Fig. 2(b) is a BPT diagram of all the sources, with the region inhabited by high-excitation galaxies marked.

VCV refers to the Véron-Cetty & Véron (1987) catalogue of active galaxies and quasars and dG to the de Grijp *et al.* (1987) catalogue of warm *IRAS* sources thought to be AGN candidates.

One galaxy in our sample, 14151+2705 (MKN 673), is listed as a Seyfert 2 in the catalogue of Markarian galaxies by Mazzarella & Balzano (1986). No emission lines are present in the spectrum of this galaxy or its companion so we are unable to support the Seyfert 2 classification.

The above list should not be considered complete as it is possible, if spectra with better signal-to-noise ratios of some galaxies were obtained, a few would also be classified as active. Seven other galaxies are within 0.1 of passing criterion (i), and, of these, six pass criterion (ii). Even if these six galaxies are classified as active, however, the fraction of high luminosity ($L_{60\mu m} > 10^{11.5} L_{\odot}$) galaxies that are active is 40 per cent, much less than the 90 per cent of Sanders *et al.* (1988). One important difference between the sample of galaxies presented here and that of Sanders *et al.* is that the mean redshift of our galaxies is greater than the mean redshift of Sanders' galaxies. A greater fraction of the galaxy will be covered by our slit and this galaxy light may overwhelm a faint active nucleus, leading to an H II region classification.

Table 3. Observed luminosities and colours of the sample galaxies.

Name	z	$Log(L_{60\mu m}/L_{\odot})$	$L_{H\alpha}$	[3800-5700]	[3800-6560]	Comments
12590+2934	0.02346±0.00001	11.32	41.42	1.91	2.37	LINER.
13005+3556 Nucl	0.03731±0.00004	11.36	41.51	1.40	1.58	
13005+3556 Plume	0.03729±0.00003		41.52	1.37	1.67	
13086+2950	0.02429±0.00004	10.87	40.73	2.24	2.68	
13111+4348	0.05789±0.00002	11.79	41.84	1.19	1.51	
13126+2452	0.01336±0.00014	11.25	39.50	1.33	1.52	
13183+3423	0.02331±0.00003	11.67	41.05	1.23	1.36	
13238+3611	0.01910±0.00003	10.97	41.14	2.03	2.31	
13257+4754	0.06103±0.00004	11.62	41.08	0.85	0.97	
13326+3417	0.02420±0.00004	10.97	41.12	1.34	1.52	
13342+2321	0.17967±0.00004	12.41	42.63	1.15	1.90	Seyfert 2; Possible broad wings
13362+4831 North	0.02842±0.00001	11.53	41.91	1.42	1.64	LINER
13362+4831 South	0.02843±0.00001		41.84	1.45	1.72	Seyfert 2
13376+2839	0.01639±0.00003	10.74	40.27	1.89	2.17	
13387+2331	0.02709±0.00002	11.33	41.21	1.73	2.04	LINER.
13387+2951	0.07776±0.00002	11.74	41.59	1.32	1.67	
13408+3035	0.03498±0.00004	11.22	41.29	1.85	2.07	
13442+2321 South	0.14165±0.00007	12.37	41.45	1.30	1.85	
13457+3513	0.11565±0.00006	11.95	41.86	1.29	1.54	
13470+3530 H II	0.01767±0.00003	11.03	41.01	1.50	1.75	
13470+3530 Nucl	0.01745±0.00004		40.48	1.93	2.26	
13532+2517	0.030	11.05				
13536+1836 East	0.05019±0.00001	11.52	42.56	0.77	1.12	Two nuclei, East is a Seyfert 2.
13539+3019	0.032	11.06				
13539+2920	0.10904±0.00003	12.18	41.98	1.64	1.99	
13564+3741	0.01173±0.00001	10.75	41.05	1.36	1.63	
13565+3519	0.03499±0.00003	10.33	41.21	1.77	2.08	
13573+2517	0.06426±0.00007	11.51	40.66	1.38	1.73	
13589+4305 South	0.03319±0.00002	11.20	41.23	1.89	2.16	
						No emission lines detected in north object.
14003+3245	0.01491±0.00003	10.94	40.87	1.88	2.24	
14008+2816	0.01561±0.00005	10.51	40.30	2.52	2.92	
14026+3058	0.02577±0.00003	11.02	40.58	1.62	1.93	
14046+3400	0.03540±0.00002	11.28	41.32	1.76	2.12	
14048+1524	0.0247	10.89				
14057+3227	0.08671±0.00004	11.86	41.71	1.25	1.57	
14060+2919	0.11700±0.00002	12.16	42.50	1.00	1.39	
14082+1347	0.01617±0.00002	10.74	40.63	2.13	2.46	Seyfert 2.
14096+2428	0.06287	11.56	38.89	1.75	2.10	
14124+1522	0.0154	10.44				
14144+3949 Arm	0.02572±0.00003	10.96	41.01	1.29	1.57	
14144+3949 Nucl			41.07	1.99	2.34	
14144+3949 Comp	0.02587±0.00007		40.74	1.53	1.78	
14151+2705 East	0.03673±0.00004	11.35	41.45	1.59	1.88	
14151+2705	0.03704±0.00007		40.85	1.11	1.28	
14158+2741	0.06966±0.00008	11.84	40.94	1.67	2.06	
14165+2510	0.01799±0.00003	10.76	40.85	2.17	2.47	
14178+4927	0.02626±0.00002	11.39	41.36	1.69	2.00	
14202+2615	0.15915±0.00003	12.41	41.12	1.03	1.55	
14203+3005	0.11445±0.00003	11.95	42.29	1.16	1.54	Seyfert 2
14221+2450	0.01727±0.00002	10.91	40.97	0	0	
14228+1358	0.01888±0.00008	10.67	39.68	2.17	2.51	
14229+1424 West	0.06158±0.00002	11.62	41.84	0.67	0.96	
14271+4203	0.01852±0.00006	10.65	38.85	1.99	2.29	
14280+3126 H II	0.01168±0.00001	10.96	41.20	0.75	0.88	
14280+3126 Nucl			40.83	0.97	1.14	
14280+3126 Arm			40.84	1.34	1.55	
14283+3532	0.01062±0.00021	10.23	40.11	1.94	2.13	
14296+2209	0.04450±0.00002	11.42	41.57	1.39	1.69	
14332+3520	0.02893±0.00002	11.15	41.43	1.06	1.19	
14356+3041 North	0.03499±0.00002	11.23	42.19	1.08	1.19	
14356+3041 South	0.03480±0.00003		41.35	1.30	1.56	
14405+2634	0.10825±0.00005	11.95	41.91	1.13	1.36	
14422+1644	0.02194±0.00008	10.75	40.47	2.50	2.85	
14434+3859	0.03262±0.00005	11.18	40.83	1.34	1.59	
14459+1745						
14471+2333 West	0.08716±0.00004	11.92	41.43	1.21	1.43	
14471+2333 East	0.08749±0.00005		41.38	1.20	1.60	
14547+2448 South	0.03295±0.00003	11.61	41.14	1.09	1.24	
14547+2448 North						
14575+3256	0.11420±0.00002	12.01	42.63	1.01	1.35	
15018+2417	0.06916±0.00006	11.95	41.33	1.32	1.70	

Notes: (1) Unless noted, all galaxies exhibit H II region-like spectra. (2) The redshift quoted is the galactocentric redshift, derived from the heliocentric velocity using a correction of $v = 300 \sin l \cos b$. (3) The Hα luminosity is given in units of log(erg s^{-1}). Luminosities are calculated using $H_0 = 50$ km s^{-1} Mpc^{-1}, $q = \frac{1}{2}$ ($\Omega = 1$) and using the galactocentric redshift.

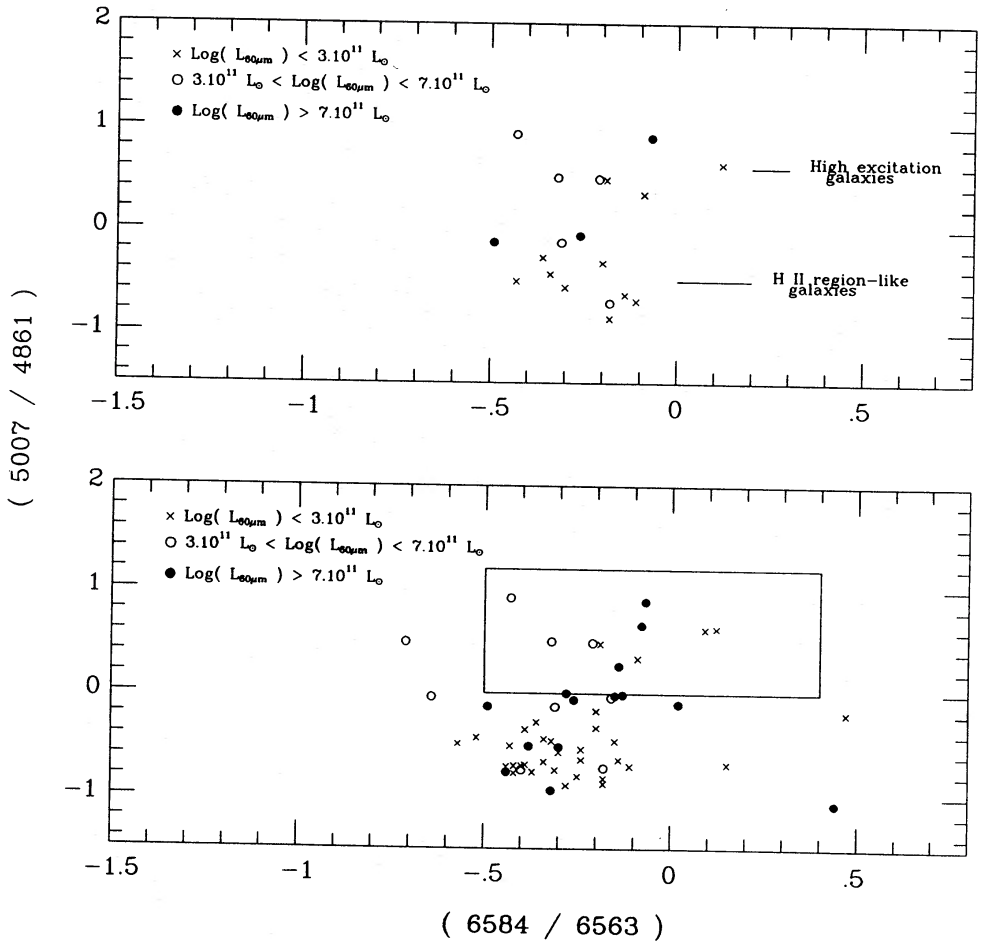

Figure 2. This shows one of the BPT diagrams used in the spectral classification of the *IRAS* galaxies. Fig. 2(a) (top) shows sources with high signal-to-noise spectra where the division between high- and low-excitation galaxies is pronounced. Fig. 2(b) shows all the *IRAS* galaxies and boxes the region inhabited by high excitation galaxies. Most, but not all, of the galaxies in this region are active. Some fail other criteria that distinguish between active and non-active galaxies.

Table 4. *IRAS* sources classified as active from line ratio diagrams.

Galaxy	Optical name	Classification	Log($L_{60\mu m}$)	$< \Delta E >$	Notes
12590+2934	NGC 4922A+B	LINER	11.32	0.39	VCV Say Sey 2
13342+3932		Seyfert	12.41	0.40	New
13362+4831 N		LINER	11.52	0.40	Agree VCV
13362+4831 S		Seyfert	11.52	0.36	Agree VCV
13387+2331	MCG 4-32-25	LINER	11.31	0.51	New
13536+1836	Mkn 463	Seyfert	11.51	0.50	Agree VCV
14082+1347	ZG 1408+13	Seyfert	10.76	0.37	Agree dG
14203+3005		Seyfert	11.94	0.55	New

5 Interpretation of line ratios and colours of the sample galaxies

5.1 EXCITATION AND ABUNDANCES

The *IRAS* galaxies have [N II]/Hα ratios in the range $\frac{1}{3}$ to 1 with an average of ≈ 0.7, consistent with solar abundances, but since we do not know the ionization parameter we cannot make a more specific statement. For most of the *IRAS* sources, the [N II]/Hα ratios are similar to the ratios found in the nuclei of late-type spirals (Keel 1983) and in French's (1980) sample of optically selected starburst galaxies. The ratios are, however, slightly higher than the value of ≈ 0.3 expected for H II regions in the outer arms of galaxies (Peimbert 1975) and smaller than the ratio of > 1 in early-type spirals (Keel 1983), usually associated with LINER-type activity.

The [O III]/Hβ ratio for *IRAS* galaxies is smaller than that of optically selected starburst galaxies. This ratio is plotted against $L_{60\mu m}$ in Fig. 3, along with optically selected starburst galaxies taken from French (1980) and Balzano (1983). Luminosities for the optically selected galaxies are calculated using the redshifts in Mazzarella & Balzano (1986) and 60-μm flux measurements from the same paper, originally listed in the *IRAS* PSC. Where a galaxy's 60-μm flux was not detected, an upper limit of 0.5 Jy was assumed. The *IRAS* galaxies have a lower [O III]/Hβ ratio, indicating lower ionization, than the optically selected starburst galaxies. Here, the corrected Hβ fluxes have been used, but any errors in the corrections are not enough to explain the difference.

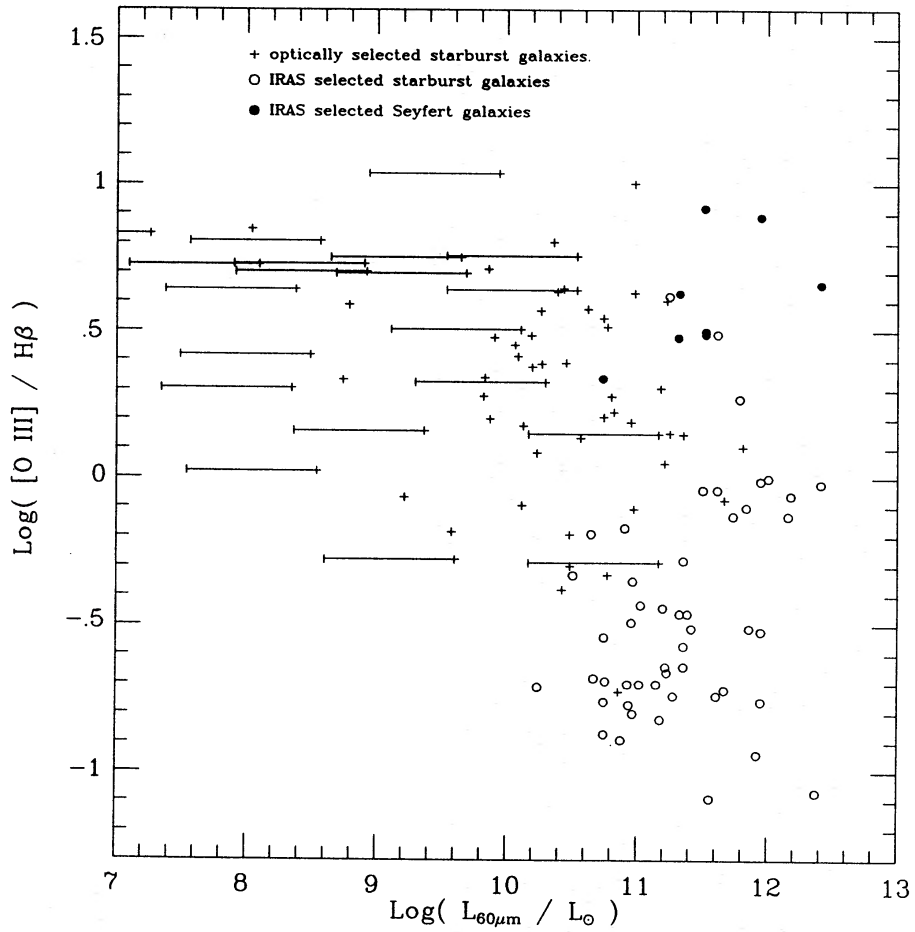

Figure 3. [O III]/Hβ ratio for *IRAS* galaxies with H II region-like spectra and optically selected 'starburst' galaxies. A horizontal line extending from a galaxy indicates an upper limit to its IR luminosity.

The lower ionization of *IRAS* galaxies was also found by Allen *et al.* (1985) in their observations of a sample of 19 optically faint *IRAS* galaxies. Sarazin (1976) (see also Sarazin 1977 and Shields & Searle 1978) discussed a possibly related result. While studying the properties of H II regions in the spiral arms of nearby galaxies, he found a relationship between H II region's ionization and its distance from the galaxy's nucleus. His measured [O III]/Hβ ratios have similar values to those found in *IRAS* galaxies. He proposed that increasing the metallicity of an H II region also increased the dust content, which resulted in smaller line ratios due to the dust competing with the gas for ionizing photons. Because of spiral galaxy abundance gradients, H II regions in their arms will have different metallicities, leading to different line ratios. Are abundances the cause of differing line ratios in *IRAS* galaxies and normal galaxies?

5.2 THE Hβ/Hα RATIO AND REDDENING OF THE GAS

Using the Hβ/Hα emission ratio, it is possible to calculate the reddening towards the emission-line region in the galaxies. Without correcting for the estimated stellar Balmer absorption from early-type stars, an average upper limit to A_v of ≈ 3.5 is found. Correcting for the estimated stellar Balmer absorption, we calculate a typical A_v towards the emission-line region of ≈ 1.0. Sixty-three per cent of the galaxies have an A_v of less than 2, 10 galaxies have an A_v in the range 2–3, five have an A_v of between 3 and 4 and two galaxies (13573+2517 and 14283+3532) have an $A_v > 4$.

An average $A_v = 1$ may reflect the fact that the dust and gaseous emission are co-distributed but clumped, such that the apparent optical emission is dominated by regions with low optical depth and anything lying 'deeper' is not seen. While this depends on the exact geometry of the emission clouds and the dust, wherever cases of A_v of about unity are found we must be aware that most of the optical light may be absorbed and that we may not be seeing the underlying energy source in the optical.

5.3 THE OPTICAL COLOURS AND REDDENING OF THE STARS

Observed [3800–5700] and [3800–6560] colours (broadly comparable to [U–V] and [U–R] colours) were derived as the ratios of monochromatic continuum fluxes expressed as magnitudes. These are plotted in Fig. 4, with different symbols representing the galaxies in each of three luminosity ranges. Also plotted are comparison points for stars (O'Connell 1973), M31 (O'Connell 1976), the average position for elliptical galaxies (O'Connell 1976), a variety of Sc galaxies (Turnrose 1976), two active galaxies and a reddening vector. These comparison points were derived from the published spectrophotometry in the same manner as for our sample galaxies.

The *IRAS* galaxies have a considerable range in colour, but follow a well-defined locus, with a definite difference between high- and low-luminosity galaxies. Most of the *IRAS* galaxies are redder than the sample of galaxies used by French (1980). The low-luminosity galaxies have the colours of bulges in spiral galaxies or of ellipticals, indicating the presence of a normal, late-type stellar population. The higher-luminosity galaxies, however, have bluer colours, similar to those of Sc galaxies or relatively young (A–F) stars. Also the very high-luminosity galaxies, those with luminosities greater than $10^{12} L_{\odot}$, tend to lie above the rest of the sample and have redder [3800–6560] colours.

The colours of most of the *IRAS* galaxies may then be synthesized by a normal stellar population. We cannot derive a unique population solution of course. In particular, the reddening vector is parallel to the stellar locus, giving an extra ambiguity in the solutions. For

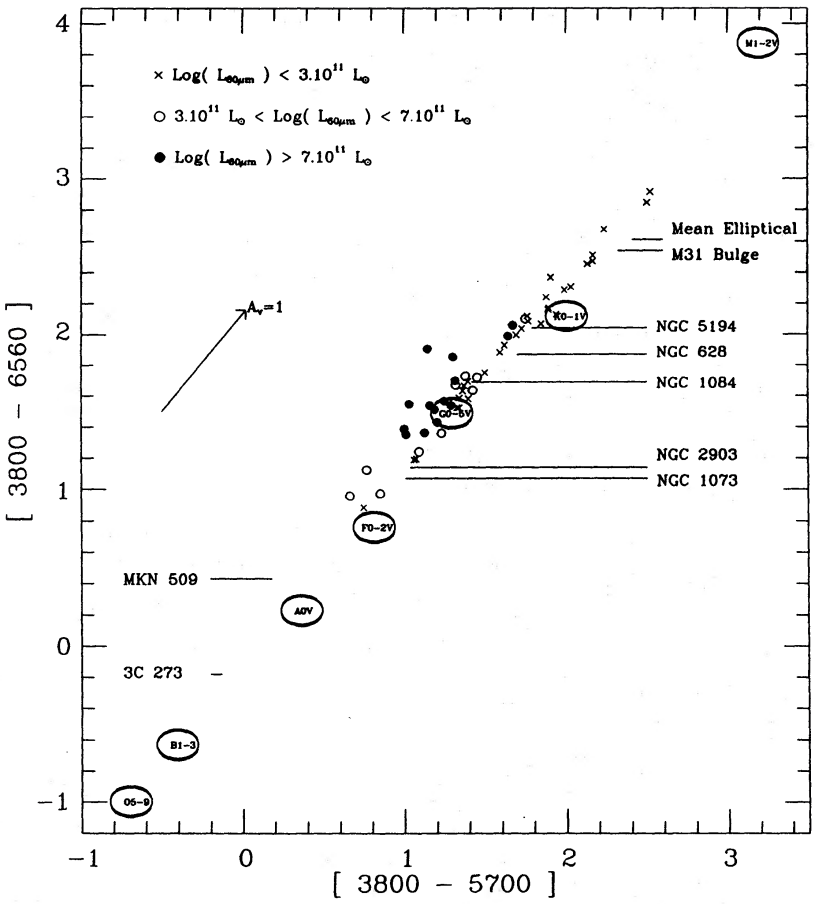

Figure 4. [3800–5700] against [3800–6560] colours for the galaxies. Comparison points of stars, normal Sc galaxies (NGC numbers) and active galaxies are given, along with a reddening vector. The higher-luminosity galaxies are bluer than the low-luminosity galaxies. The colours have not been corrected for reddening.

example, some colours could be explained as being dominated by OB stars with $A_v = 3$, or more naturally, by lightly reddened AF stars. In Section 6.6 we discuss further the question of how many OB stars may be present.

Some galaxies, however, lie well above the stellar/reddening locus and could be alternatively explained as containing a reddened AGN, possibly mixed with late-type starlight. Some of these objects are not spectroscopically classified as active galaxies and so are candidates for obscured AGN. These galaxies are 13442+2321, 14060+2919, 14202+2615, 14229+1428 and 14575+3256. Some of the objects that are spectroscopically classified as active have colours consistent with either starlight or reddened AGN; there is a range of AGN colours and, in particular, 3C 273 looks little different from a hot star in these colours.

We observed many galaxies to have strong Balmer absorption. The light from these is presumably dominated by the light from AF stars, but to place these galaxies in the AF region of the colour–colour diagram needs slightly more de-reddening than is implied by the Hα/Hβ ratio. This suggests that the extinction towards young stars is slightly greater than towards the emitting regions.

The strength of the Hα emission line is correlated with the galaxy colour. Fig. 5 plots log(Hα equivalent width) for the non-AGN *IRAS* galaxies against [3800–5700] colours. The bluest galaxies have the strongest Hα emission line. The two galaxies with log(Hα ew) ≈ -1 are 14271+4203 and 14096+2428. The apparent weakness of their Hα line is discussed further in Section 6.4.

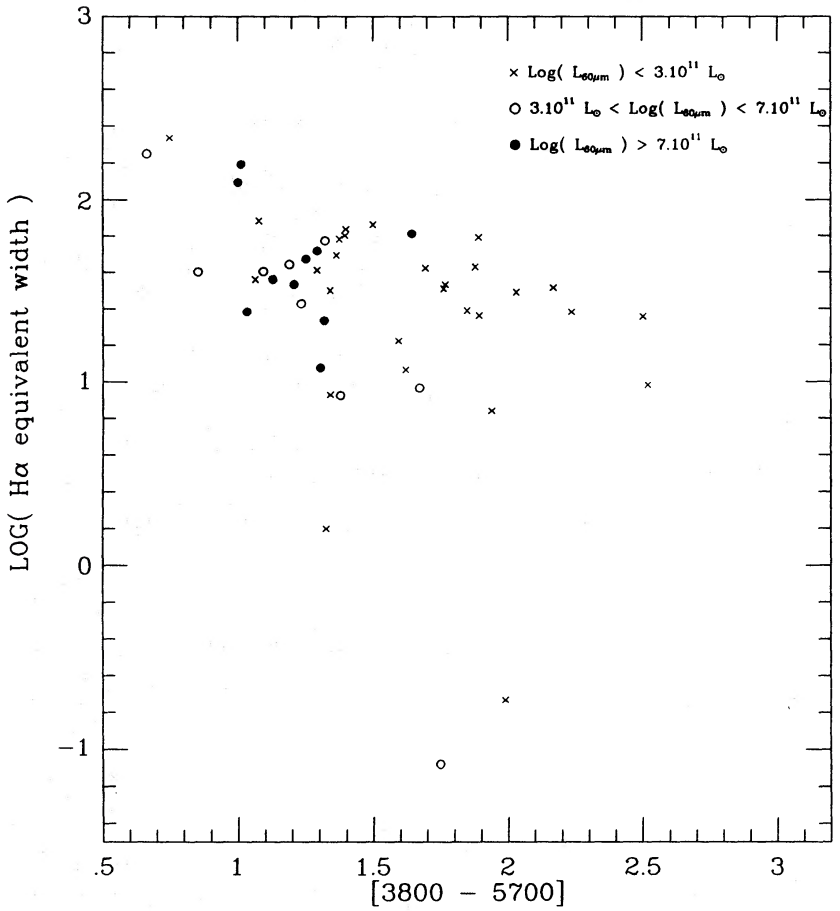

Figure 5. Log(Hα) equivalent width against [3800–5700] colour for the *IRAS* galaxies excluding active galaxies. Strong emission lines are correlated with blue colours. The two galaxies with log(Hα ew) about -1, 14271+4203 and 14096+2428, are also discussed in Section 6.4.

6 Discussion

6.1 THE PROPORTION OF INTERACTING AND ACTIVE GALAXIES

Combining the results of this paper and Paper I, it is possible to determine the proportion of interacting and active galaxies as a function of IR luminosity. This is shown in Fig. 6 for the two flux-limited groups in the sample. Fifty-six of the 61 sample *IRAS* sources are included (five were not observed with the IPCS). As noted, the sample of sources with luminosities below $10^{11.5}L_{\odot}$ is 86 per cent complete and the sample of sources with luminosities above this value is 97 per cent complete. Interacting sources are defined as *IRAS* sources with optical counterparts showing evidence for an interaction with a companion, such as tidal arms or bridges. Grossly irregular structure, or two nuclei in the same common envelope, would suggest a merger. The fraction of unusual galaxies (i.e. galaxies which are interacting or exhibit spectra consistent with coming from an AGN) in each of four luminosity ranges, split to have approximately equal numbers of sources in each, are shown in Table 5.

About 15 per cent of optically selected spiral galaxies are interacting (Paper I; Armus, Heckman & Miley 1987) and 5 per cent are active (Keel 1983). These are approximately the same fractions as found in the lowest IR luminosity group. The next two luminosity groups contain approximately the same fraction of interacting or active galaxies, with just under half the *IRAS* sources being unusual, while the highest luminosity group is heavily biased towards interacting systems and active galaxies. The probability of an *IRAS* galaxy being an active

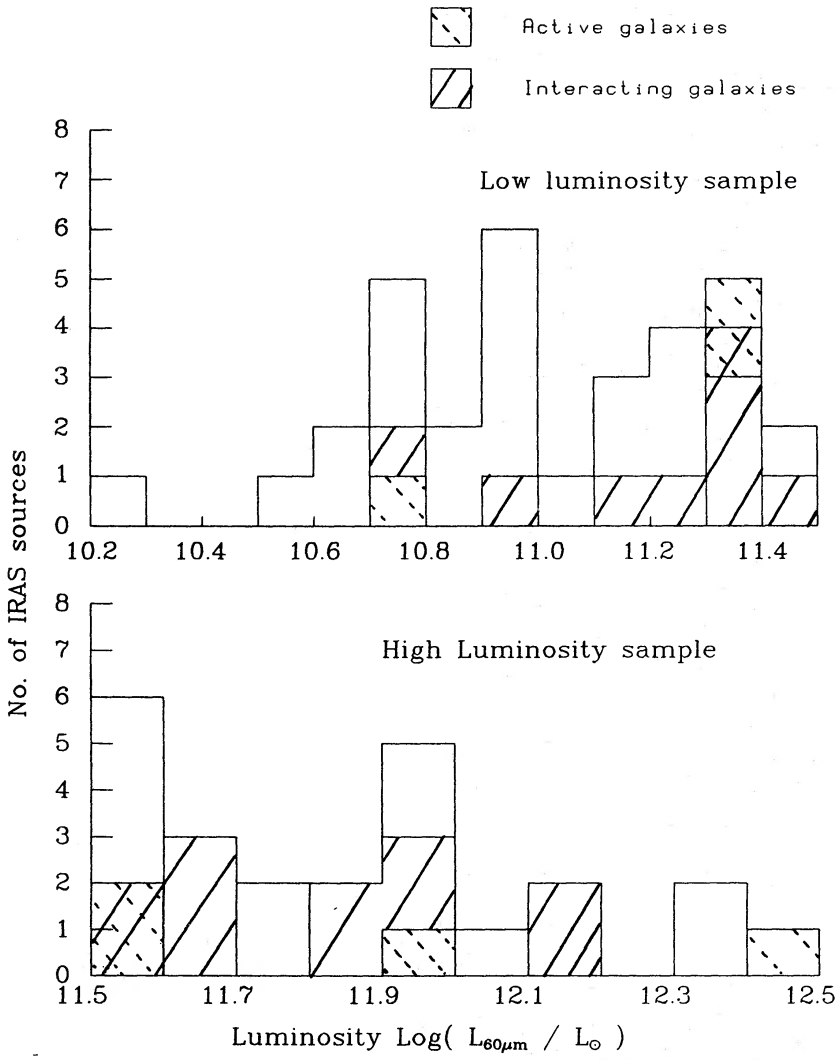

Figure 6. Combined results of this paper and Lawrence *et al.* (1989) showing the numbers of interacting and active galaxies as a function of luminosity.

Table 5. The fractions of unusual galaxies in four luminosity ranges.

Luminosity range	No. of Sources	No. only Interacting	No. only Active	Number active & Interacting	Number Unusual	Notes
$\text{Log}(L_{60\mu m}/L_\odot)<11$	17	2 (12%)	1 (6%)		3 (18%)	2Jy group
$11<\text{Log}(L_{60\mu m}/L_\odot)<11.5$	15	6 (40%)	1 (7%)	1 (7%)	8 (53%)	2Jy group
$11.5<\text{Log}(L_{60\mu m}/L_\odot)<11.8$	11	3 (27%)		2 (18%)	5 (45%)	1Jy group
$\text{Log}(L_{60\mu m}/L_\odot)>11.8$	13	6 (46%)	2 (16%)		8 (62%)	1Jy group

galaxy does not appear to be a function of the galaxy's IR luminosity. The fraction of active galaxies in our sample is approximately the same as in optically selected samples (Keel 1983). We must, however, be careful when drawing conclusions from such small numbers of objects.

This conclusion can be compared with that reached by Sanders *et al.* (1988) in their survey of galaxies from the *IRAS Bright Galaxy Catalog* (see also Sanders *et al.* 1986). They surveyed 170 galaxies with IR luminosities in the range 10^{10} to greater than $10^{12}L_\odot$ (their IR

luminosities were based on the 8- to 1000-μm flux) and concluded that most of the low-luminosity galaxies were normal, showing no signs of interaction or of having an AGN ionization source. The fraction of interacting galaxies or galaxies exhibiting evidence for an AGN increased with luminosity, and all 10 galaxies having luminosities greater than $10^{12}L_{\odot}$ were strongly interacting, with nine also showing signs of having an AGN ionization source. They concluded that ultraluminous *IRAS* sources were spiral galaxies undergoing mergers. The initial merger caused the formation of stars, leading to the objects being classified as starbursts, but it also fed any AGN in the galaxies. Eventually the starburst would die out, leaving the AGN as the dominant energy source.

The data presented in this paper do not support this as a unique model explaining all high-luminosity *IRAS* galaxies. There are apparently solitary, undisturbed galaxies, with luminosities greater than $10^{12}L_{\odot}$, showing no signs of interaction or AGN activity. 14575+3256 is a solitary galaxy, while 13442+2321 and 14202+2615 have neighbours but show no signs of interaction with them. As potential counter-examples whose high IR luminosity has no apparent cause, these galaxies should be studied further, although we note that it is dangerous to search for peculiarities only where one expects to find them!

It should be noted that the majority of interacting galaxies in this sample have optical spectra like those of H II regions. In an *IRAS*-selected group of galaxies, interactions, in general, are associated with star formation and not AGN. Whether any AGN present in the interacting galaxies classified as starburst will eventually dominate the energy output, as in the theory by Sanders *et al.*, is unknown. While it is believed that interactions do trigger star formation (e.g. Larson & Tinsley 1978; Roos 1981; Byrd *et al.* 1986), there is considerable discussion as to the role of interactions as the trigger of Seyfert activity in galaxies (see, for example, the review by Balick & Heckman 1982).

6.2 INTERACTING AND NON-INTERACTING GALAXIES: IS THERE A SPECTROSCOPIC DIFFERENCE?

There was no obvious distinction in the line ratio diagrams between interacting and non-interacting galaxies. There also seemed to be no difference in the ratio of $S_{100\mu m}/S_{60\mu m}$ at a given $L_{60\mu m}$. A more hopeful possibility was that the interacting galaxies may have broader emission lines. Fig. 7 is a histogram of the Hα and [N II] FWHM linewidths, uncorrected for instrumental broadening, for the H II region-like galaxies (active galaxies have been excluded because of their broad emission-lines). The galaxies are split into two groups: those which are thought to be interacting and those believed not to be. The galaxies classified as interacting may have greater linewidths than those classified as non-interacting, but the effect has a low statistical significance. A Kolmogorov–Smirnov test showed that there is no significant difference between the distribution of Hα and [N II] linewidths for the two groups. Finally, we examined the strength of line emission by examining the Hα+[N II] equivalent width distribution and the Hα equivalent width distributions. Again there is no significant difference between interacting and non-interacting galaxies.

This seems to contradict the study by Kennicutt *et al.* (1987), who discussed the effect of interactions on the properties of optically-selected galaxies and briefly reviewed previous work on the subject. They claimed that there was a strong correlation between the strength of the Hα emission and whether a galaxy was interacting. They, however, surveyed a sample of optically-selected Arp galaxies heavily biased towards strongly interacting systems, whereas our IR-selected sample contains mostly relatively weakly interacting galaxies. It is possible that the spectroscopic properties of strongly interacting systems are different from non-interacting systems, but most interacting galaxies detected by *IRAS* do not have spectroscopic properties very different from those of solitary galaxies with strong emission lines.

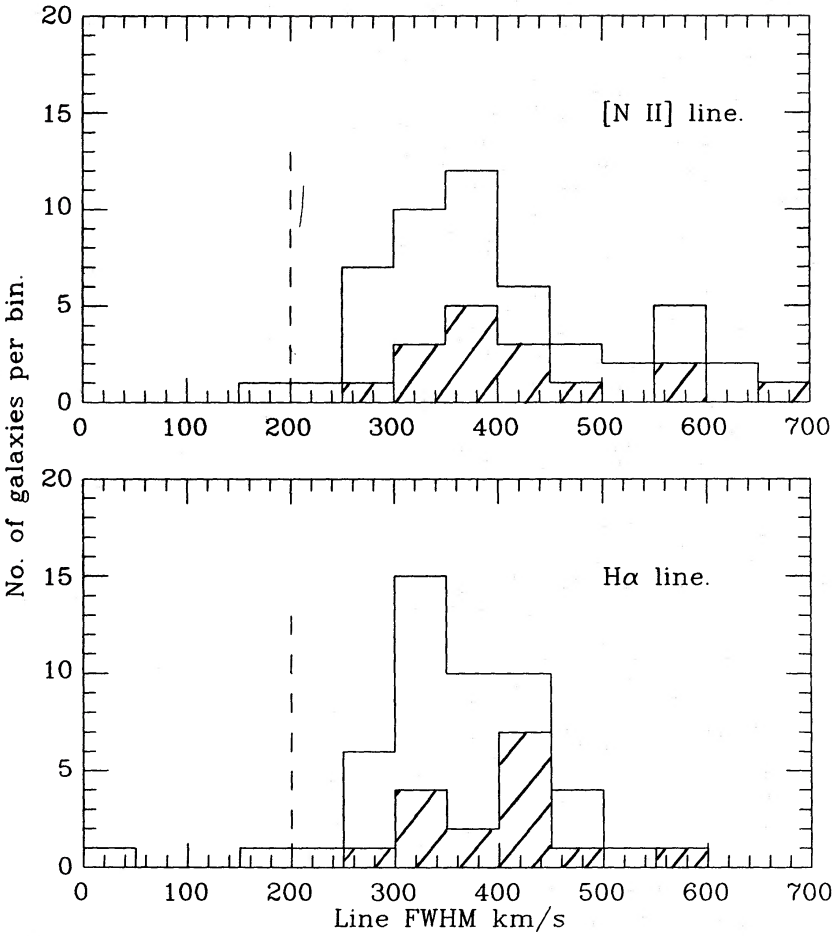

Figure 7. Hα and [N II] (FWHM) linewidths for interacting (shaded) and non-interacting (unshaded) *IRAS* galaxies, excluding active galaxies. There is no significant difference between the linewidths of the interacting and non-interacting galaxies. The instrumental resolution (FWHM) is indicated by the dashed line.

6.3 *IRAS* ACTIVE GALAXIES

We shall only make a few simple points about the active galaxies. First, all the Seyferts are of Type 2. In general, *IRAS* finds Seyferts of Type 2 with several times the frequency of Type 1. This is consistent with the idea that Type 2 Seyferts are obscured by dust and that this is a global, rather than a line-of-sight, effect (e.g. Lawrence 1987 and references therein). The second point is that, from the ratio of $S_{60\mu m}/S_{25\mu m}$, they are particularly warm. Five out of seven of our active galaxy *IRAS* sources would fail the criterion of de Grijp *et al.* (1987), that is, $\alpha_{60-25} < 1.5$. On the other hand, α_{100-60} is typically very warm; six out of seven have $\alpha_{100-60} < 0.07$ and three out of seven have $\alpha_{100-60} < 0.0$. This strong spectral curvature over 25–60–100 μm indicates that the general *IRAS*-selected active galaxy is dominated by a thermal component peaking at about 60 μm. Finally, we note that the ratio $L_{60\mu m}/L_{H\alpha}$ is typically several thousand, whereas for Type 1 Seyferts it is normally a few hundred (Ward *et al.* 1987; Edelson & Malkan 1986). Again, this suggests a strong thermal component in the *IRAS* Type 2 Seyferts which is relatively rare in Type 1 Seyferts.

6.4 THE $L_{60\mu m}$ TO $L_{H\alpha}$ RATIO FOR H II REGION-LIKE GALAXIES

Fig. 8 is a plot of $L_{H\alpha}$ against $L_{60\mu m}$ for the *IRAS* starburst galaxies. Interacting galaxies, where some Hα emission may have been missed, and active galaxies, which have a different energy source, have been excluded. The galaxies have $L_{60\mu m}/L_{H\alpha} \simeq 4000$, greater than the ratio of

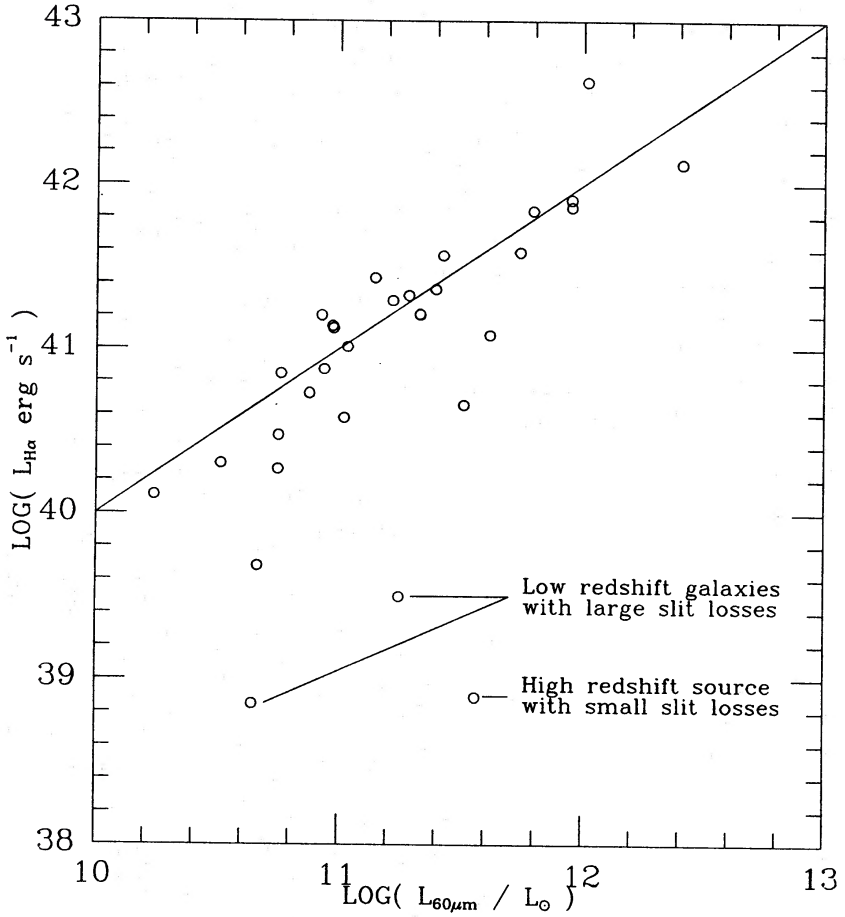

Figure 8. Hα luminosity against IR luminosity for *IRAS* galaxies, excluding active or interacting systems. There is a much tighter correlation than for all the galaxies. The line drawn corresponds to $L_{60\mu m}/L_{H\alpha}=4000$. No extinction correction has been made to Hα.

20–200 found in the discs of bright spiral galaxies (Persson & Helou 1987). If we correct Hα for extinction based on the Hβ/Hα ratio, the $L_{60\mu m}/L_{H\alpha}$ ratio changes typically by a factor of 2–3, insufficient to explain the difference with normal spiral discs. As discussed in Section 5.2, however, the extinction correction is almost certainly an underestimate [note that Persson & Helou (1987) use Hα fluxes with the extinction corrected using radio data]. Fig. 8 shows a much tighter correlation than for *IRAS* galaxies in general (*cf.* fig. 7 of Leech *et al.* 1988). There is still, however, considerable scatter in the diagram, greater than the expected errors, which must signal a real physical difference amongst the galaxies – probably a difference in the optical depth of the starburst. In Section 6.6, we discuss the fact that simple models with uniform optical depth cannot simultaneously explain the Hβ/Hα and $L_{60\mu m}/L_{H\alpha}$ ratios, and present a more sophisticated and successful model.

While the majority of the galaxies have a $L_{60\mu m}/L_{H\alpha}$ ratio of about 4000, some have a much larger ratio. Examples of such galaxies include 13126+2452, 14271+4203 and 14283+3532. No Hα emission was detected from 14224+1358, although it is an edge-on spiral and so may be heavily reddened in the line-of-sight. Nearby galaxies would be expected to have a higher $L_{60\mu m}/L_{H\alpha}$ ratio (i.e. lie below the line) because, while *IRAS* detects all their IR flux (one of the selection criteria was that they had to be point sources), they have a larger angular size than the slit used to determine their Hα flux, leading to an underestimate of $L_{H\alpha}$. 14271+4203 and 13126+2452 are nearby galaxies with redshifts of ≈ 0.015. Assuming the Hα emission to cover the whole galaxy and to be distributed like starlight, then, taking the growth curve of Griersmith, Hyland & Jones (1982) and a galaxy diameter of 20 kpc, we

estimate that the Hα flux could have been underestimated by a factor of 10, bringing their IR to Hα ratios nearer to those of other galaxies. This effect does not account for the large ratios seen in some of the more distant galaxies. 14096+2428 has a redshift of 0.063, so a 1.5-arcsec wide slit would not be expected to lose more than about ≈ 80 per cent of the Hα emission. Multiplication of the observed Hα emission by 5 still leads to an IR to Hα ratio of greater than 40000 (to achieve a $L_{60\mu m}/L_{H\alpha}$ ratio of 4000, in line with the other galaxies, we must assume that more than 99 per cent of the Hα emission was lost compared to the other *IRAS*-selected starburst objects). What is this *IRAS* source and what is 14224+1358, a galaxy with no detected Hα emission? They are not cirrus (the IR colours are wrong) and the galaxy identifications seem reasonable on positional grounds (Lawrence *et al.* 1986). Naively, such high $L_{60\mu m}/L_{H\alpha}$ ratios may be explained by galaxies and/or starburst regions which are generally more dusty. In the light of the discussion in Section 6.6 however, it is likely that they are younger starbursts, with the majority of OB stars still completely buried in their parent molecular clouds.

6.5 DO THE OBSERVED O STARS ACCOUNT FOR THE IR OR LINE EMISSION?

As discussed in Section 5.3, the high-luminosity galaxies have a range of colours similar to those seen in nearby Sc galaxies. In principle, one could model the number of stars of various spectral types which are present, using colours and absorption indices, but we do not have the necessary data. Instead, we use models of Turnrose (1976) for galaxies of similar colour, and scale by the observed $\lambda 5450$ flux, to obtain the number of ionizing stars (O5–9) likely to be present. We then assume, as did Turnrose, that each star in the range O5–9 produces 10^{49} ionizing photons. We next assume that 2.2 ionizing photons produce 1 Hα photon (Osterbrock 1974). The net effect is to produce a predicted relation between $L_{H\alpha}$ and L_{5450}. We performed this calculation for seven different models from Turnrose (1976), covering a range of observed colours, and compared the results with the observed correlation between $L_{H\alpha}$ and L_{5450} for our *IRAS* sample (not shown here). The range of predicted relations (covering approximately a factor of 10 in $L_{H\alpha}/L_{5450}$) agrees well with the observed correlation and its scatter, except that 20 per cent of the *IRAS* galaxies have $L_{H\alpha}/L_{5450}$ up to a factor of 2–3 greater than any of the models.

There are, of course, considerable uncertainties in these calculations, but to first order it seems that the observable hot stars do account for the observed line-emission. We may similarly ask if the implied O-star luminosity is compatible with the IR luminosity. Assuming the stellar radiation to be approximately blackbody, and the reddening to be small, we can calculate the expected $L(\text{total})/N(\text{ionizing photons})$, which gives an upper limit to $L_{60\mu m}/L_{H\alpha}$. For O5–9 stars this ratio is ≈ 50, which leaves $L_{60\mu m}/L_{H\alpha}$ two orders of magnitude short of the typical observed $L_{60\mu m}/L_{H\alpha}$. Of course, dust may be heated by stars of all other kinds accompanying the O stars. However, for any reasonable IMF (e.g. Salpeter 1955; Miller & Scalo 1979) we find that the total luminosity increases by, at most, a factor of a few, unless we use a very low high-mass cut-off. The total mass required to explain objects of $L_{60\mu m} \approx 10^{12} L_{\odot}$ then becomes embarrassingly high. Rather than explore this in any detail, we follow the possibility of star-formation regions with high optical depths, as detailed in the following section.

6.6 A SIMPLE MODEL FOR THE STAR-FORMING REGIONS IN HIGH-LUMINOSITY *IRAS* GALAXIES

We first summarize some salient features of the observations

(i) The observed optical emission line ratios correspond to $A_v \approx 1$.

(ii) The number of ionizing stars implied by the optical colours is consistent with the observed emission-line luminosity.

(iii) The far-IR colours are consistent with star-forming regions of much higher optical depth, $A_v \approx 20$ (Rowan-Robinson & Crawford 1986, 1989).

(iv) Likewise, the large observed ratio of $L_{60\mu m}/L_{H\alpha}$ implies a region of large optical depth. Reddening as large as $A_v \approx 20$, however, would result in virtually no observable Hα emission.

The simplest consistent model (Crawford, in preparation), is to postulate two types of cloud: (i) High optical depth clouds ('Type-I') corresponding to regions of very high-mass star formation. These are required by the infrared spectrum of starburst regions (Rowan-Robinson & Crawford 1986, 1989), and by the very high $L_{60\mu m}/L_{H\alpha}$ values found in the present work. (ii) Clouds of much lower optical depth ('Type-II') to account for the optical continuum and line emission from the galaxies. We take the optical depth of these clouds to be that implied by the observed Hα/Hβ ratio. A suitable mix with Type-I clouds will yield the observed $L_{60\mu m}/L_{H\alpha}$. Since there is essentially no contribution to the emission line flux from the Type-I clouds, we can use our adopted value for the optical depth in the Type-II clouds to de-redden the observed Hα flux from the galaxy, with the dust competition for ionizing photons left as a parameter. On the assumption that the Type-I and Type-II clouds contain stars described by the same IMF, the ratio of the luminosities generated by the two types of cloud is predicted to be

$$\frac{L_{\rm I}}{L_{\rm II}} = 0.355 \times F \frac{L_{60\mu m}}{L_{H\alpha}} \times \left(\frac{H\alpha}{H\beta}\right)^{-2.5} - 1,$$

where F is the fraction of ionizing photons absorbed by the gas in the Type-II clouds (Crawford, in preparation). If we adopt $F \approx 70$ per cent, as representing the values deduced for giant H II regions in our Galaxy (Smith, Biermann & Mezger 1978) and assumed by Belfort, Mochkovitch & Dennefeld (1987) in their models for starburst galaxies, then we find that, in all but three cases, the Type-I clouds dominate the emission in the infrared. The wavelength at which the bulk of the energy from the Type-II clouds is emitted will depend on the proximity of the dust to the stars. If the inner edge of the dust is driven out by expansion of the embedded H II region, then it is possible that the emission would be cool enough to be included in the 'disc' component of Rowan-Robinson & Crawford (1986, 1989). In this respect it is interesting that they found galaxies with the most dominant 'starburst' components often have an anomalously high luminosity in the 'disc' component, inconsistent with re-emission of starlight by interstellar dust. This may be evident for a contribution from cooler Type-II clouds which have a higher $L_{60\mu m}/L_{opt}$ than the optically thin interstellar medium.

Our results are summarized in Fig. 9, where lines of constant $(L_{\rm II}/L_{\rm II}+1)F^{-1}$ have been drawn, and galaxies with luminosities above and below $10^{11.5}L_\odot$ have been distinguished. Along the lines of constant $L_{\rm I}/L_{\rm II}$, objects differ in the optical depth of the Type II clouds. Noticeably, objects with high $L_{60\mu m}/L_{H\alpha}$ (>5000) tend to have low ratios Hα/Hβ, for which there is no obvious *a priori* reason.

In our picture, galaxies with $L_{60\mu m}/L_{H\alpha} > 5000$ are probably extremely young starbursts. Practically all the infrared luminosity originates from regions of very recent high-mass star formation, with $A_v \approx 20$. Little or no Hα emission will be contributed by the burst, and the observed Hα/Hβ ratio reflects the underlying 'normal' star-forming population. For galaxies with $L_{60\mu m}/L_{H\alpha} < 5000$, the starburst is more evolved and it should not be surprising that most of the galaxies are found in this state. Although the infrared luminosity is still dominated by the young star-forming regions, a significant fraction of the radiant energy is shared with clouds of

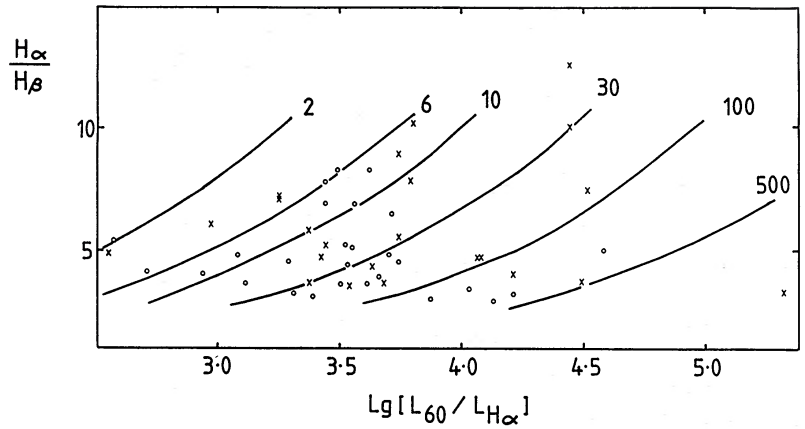

Figure 9. This is a plot of $H\alpha/H\beta$ versus $\log(L_{60\mu m}/L_{H\alpha})$ for the galaxies listed in Table 2. Galaxies having $H\alpha/H\beta$ less than 2.8 are inconsistent with the assumption of case B recombination assumed in the model and have been omitted from the diagram. Galaxies with $\log(L_{60\mu m})>11.5$ are denoted by x, those with $\log(L_{60\mu m})<11.5$ are denoted by o. The solid curves represent lines of constant $(L_I/L_{II}+1)F^{-1}$ with values indicated.

substantially lower optical depth (Type-II), whose emission-line flux dominates over the underlying 'normal' star-forming regions.

Young starburst galaxies should have strong maser emission per unit far-infrared luminosity of the galaxy and we therefore predict that this should correlate with $L_{60\mu m}/L_{H\alpha}$. Furthermore, if galaxy interactions are the direct cause of starburst activity, we would expect some correlation of structure with $L_{60\mu m}/L_{H\alpha}$.

7 Conclusions

(i) The majority of high-luminosity *IRAS* sources have H II region-like spectra, but we have found 7/56 objects which contain active galactic nuclei.

(ii) For the H II region-like galaxies, the excitation ([O III]/Hβ) is lower than that typically found in optically-selected starburst galaxies.

(iii) The $H\alpha/H\beta$ ratio implies that the (apparent) reddening towards the emission-line gas is typically $A_v \approx 1$.

(iv) Optical colours of the relatively low-luminosity objects suggest the light is dominated by a normal old stellar population. The high-luminosity galaxies generally have colours like Sc galaxies, consistent with recent star-formation. The colours of some of the high-luminosity sources, however, suggest an obscured active nucleus, including some cases where this is not apparent in the emission lines.

(v) About half of the high-luminosity objects seem to be interacting systems. Conversely, a substantial number of objects seem to be neither interacting galaxies, nor active galactic nuclei. The reason for the large luminosity of such objects is worth further study.

(vi) There is no obvious spectroscopic difference between starburst in interacting and non-interacting systems.

(vii) The IR/Hα ratio is much larger than expected for a star-forming region with $A_v \approx 1$, suggesting a much higher optical depth, whereas the visible O stars and the emission line flux are consistent with each other. A few galaxies have extreme values of IR/Hα.

(viii) To explain the observed $L_{60\mu m}/L_{H\alpha}$ and $H\alpha/H\beta$ consistently, we present a simple model with regions of two types: Type I clouds with $A_v \approx 20$, and Type II with $A_v \approx 1$. We expect that objects with large $L_{60\mu m}/L_{H\alpha}$ are the youngest starbursts, dominated by Type I clouds, i.e. by O stars still deeply embedded in their parent molecular clouds.

Acknowledgments

We thank the staff of the Isaac Newton Telescope which is operated by the Royal Greenwich Observatory at the Spanish Observatorio del Roque de los Muchachos of the Instituto de Astrofísica de Canarias, for their expert and friendly assistance. KJL acknowledges an SERC studentship and AL an SERC grant provided for *IRAS* studies.

References

Allen, D. A., Roche, P. F. & Norris, R. P., 1985. *Mon. Not. R. astr. Soc.*, **213,** 67P.
Armus, L., Heckman, T. & Miley, G., 1987. *Astr. J.*, **94**, 831.
Baldwin, J. A., Phillips, M. M. & Terlevich, R. (BPT), 1981. *Publs astr. Soc. Pacif.*, **93,** 5.
Balick, B. & Heckman, T. M., 1982. *Ann. Rev. Astr. Astrophys.*, **20,** 431.
Balzano, V. A., 1983. *Astrophys. J.*, **268,** 602.
Becklin, E. E., 1986. *The Observatory,* **106,** 57.
Belfort, P., Mochkovitch, R. & Dennefeld, M., 1987. *Astr. Astrophys.*, **176,** 1.
Byrd, G. G., Valtonen, M. T., Sundelius, B. & Valtaoja, L., 1986. *Astr. Astrophys.*, **166,** 75.
Carter, D., 1985. *Astr. Express,* **1**, 61.
de Grijp, M. H. K., Miley, G. K., Lub, J. & de Jong, T., 1985. *Nature,* **314,** 21.
de Grijp, M. H. K., Miley, G. K. & Lub, J., 1987. *Astr. Astrophys. Suppl.*, **70,** 95.
de Jong, T., Clegg, P. E., Soifer, B. T., Rowan-Robinson, M., Habing, H. J., Houck, J. R., Aumann, H. H. & Raimond, E. 1984. *Astrophys. J.*, **278,** L67.
de Poy, D. L., Becklin, E. E. & Wynn-Williams, C. G., 1986. *Asrophys. J.*, **307,** 116.
de Robertis, M. M. & Osterbrock, D. E., 1985. *Publs astr. Soc. Pacif.*, **97,** 1129.
Edelson, R. A. & Malkan, M. A., 1986. *Astrophys. J.*, **308,** 59.
Elston, R., Cornell, M. E. & Lebofsky, M. J., 1985. *Astrophys. J.*, **296,** 106.
French, H. B., 1980. *Astrophys. J.*, **240,** 41.
Griersmith, D., Hyland, A. R. & Jones, T. J., 1982. *Astr. J.*, **87,** 1106.
Harwit, M., Houck, J. R., Soifer, B. T. & Palumbo, G. G. C., 1987. *Astrophys. J.*, **315,** 28.
Hawarden, T. G., Fairclough, J. H., Joseph, R. D., Leggett, S. K. & Mountain, C. M., 1986. In: *Light on Dark Matter,* p. 455, ed. Israel, F. P., Reidel, Dordrecht.
Keel, W. C., 1983. *Astrophys. J.*, **52,** 229.
Kennicutt, R. C., Keel, W. C., van der Hulst, J. M., Hummel, E. & Roettiger, K. A., 1987. *Astr. J.*, **93,** 1101.
Larson, R. B. & Tinsley, B. M., 1978. *Astrophys. J.*, **219,** 46.
Lawrence, A., 1987. *Publs astr. Soc. Pacif.*, **99,** 309.
Lawrence, A., Walker, D., Rowan-Robinson, M., Leech, K. J. & Penston, M. V., 1986. *Mon. Not. R. astr. Soc.*, **219,** 687.
Lawrence, A., Rowan-Robinson, M., Leech, K., Jones, D. H. P. & Well, J. V., 1989. *Mon. Not. R. astr. Soc.*, **240,** 329 (Paper I).
Leech, K. J., Lawrence, A., Rowan-Robinson, M., Walker, D. & Penston, M. V., 1988. *Mon. Not. R. astr. Soc.*, **231,** 977.
McCall, M. L., Rybski, P. M. & Shields, G. A., 1985. *Astrophys. J. Suppl.*, **57,** 1.
Mazzarella, J. M. & Balzano, V. A., 1986. *Astrophys. J. Suppl.*, **62,** 751.
Miller, G. E. & Scalo, J. M., 1979. *Astrophys. J. Suppl.*, **41,** 513.
Norris, R. P. *et al.*, 1985. *Mon. Not. R. astr. Soc.*, **213,** 821.
O'Connell, R. W., 1973. *Astr. J.*, **78,** 1074.
O'Connell, R. W., 1976. *Astrophys. J.*, **206,** 370.
Osterbrock, D. E., 1974. *Astrophysics of Gaseous Nebulae,* W. H. Freeman & Co., San Francisco.
Peimbert, M., 1975. *Ann. Rev. Astr. Astrophys.*, **13,** p. 122.
Persson, C. J. & Helou, G., 1987. *Astrophys. J.*, **314,** 513.
Roos, N., 1981. *Astr. Astrophys.*, **104,** 218.
Rowan-Robinson, M. & Crawford, J., 1986. In: *Light on Dark Matter,* p. 421, ed. Israel, F. P., Reidel, Dordrecht.
Rowan-Robinson, M. & Crawford, J., 1989. *Mon. Not. R. astr. Soc.*, **238,** 523.
Salpeter, E. E., 1955. *Astrophys. J.*, **121,** 161.
Sanders, D. B., Scoville, N. Z., Young, J. S., Soifer, B. T., Schloerb, F. P., Rice, W. L. & Danielson, G. E., 1986. *Astrophys. J.*, **305,** L45.
Sanders, D. B., Soifer, B. T., Elias, J. H., Madore, B. F., Matthews, K., Neugebauer, G. & Scoville, N. Z., 1988. *Astrophys. J.*, **325,** 74.

Sarazin, C. L., 1976. *Astrophys. J.,* **208,** 323.
Sarazin, C. L., 1977. *Astrophys. J.,* **211,** 772.
Savage, B. D. & Mathis, J. S., 1979. *Ann. Rev. Astr. Astrophys.,* **17,** 73.
Shields, G. A. & Searle, L., 1978. *Astrophys. J.,* **222,** 821.
Smith, B. J., Kleinmann, S. G., Huchra, J. P. & Low, F., 1987. *Astrophys. J.,* **318,** 161.
Smith, L. F., Biermann, P. & Mezger, P. G., 1978. *Astr. Astrophys.,* **66,** 65.
Soifer, B. T. *et al.,* 1984a. *Astrophys. J.,* **278,** L71.
Soifer, B. T., Helou, G., Lonsdale, C. J., Neugebauer, G., Hacking, P., Houck, J. R., Low, F. J., Rice, W. & Rowan-Robinson, M., 1984b. *Astrophys. J.,* **283,** L1.
Soifer, B. T., Sanders, D. B., Neugebauer, G., Danielson, G. E., Lonsdale, C. J., Madore, B. F. & Persson, S. E., 1986. *Astrophys. J.,* **303,** L41.
Turnrose, B. E., 1976. *Astrophys. J.,* **210,** 33.
Véron-Cetty, M.-P. & Véron, P., 1987. *ESO Scientific Report No. 4: A Catalogue of Quasars and Active Nuclei,* 3rd edn, Munich, ESO.
Ward, M., Elvis, M., Fabbiano, G., Carleton, N. P., Wilner, S. P. & Lawrence, A., 1987. *Astrophys. J.,* **315,** 74.